Robust Astronomical Imaging Under Coexistence With Wireless Communications

Shuimei Zhang, Yujie Gu, Ben Wang, and Yimin D. Zhang

Department of Electrical and Computer Engineering
Temple University, Philadelphia, PA 19122, USA

Abstract—**Astronomical signals are extremely weak and vulnerable to radio frequency interference. To meet the increasing demand for spectrum resources, development of spectrum-sharing and interference-immune radio astronomical technologies become very important and emerging. In this paper, we develop a robust astronomical imaging technique in the presence of wireless communication interference signals. The proposed technique effectively mitigates interference signals through robust adaptive beamforming which accounts for steering vector mismatching. Simulation results demonstrate the effectiveness of the proposed method.**

keywords: Adaptive beamforming, astronomical imaging, radio interference, robust beamforming, synthetic aperture.

I. INTRODUCTION

Radio astronomy benefits the society by exploring, understanding, and explaining the origin and nature of life in the universe [1]. Radio astronomical signals span a broad frequency range between 10 MHz and 1,000 GHz and certain frequency bands are for exclusive use of radio astronomy. The radio spectrum is finite and becomes increasingly precious for astronomical observations as well as for other wireless users [2]. Nowadays, with the increasing of new wireless applications, more spectrum is required than before. For example, the GSM coalition estimates that an additional 1.8 GHz of spectrum will be needed by 2020 [3]. One of the measures being considered for effective spectrum utilization is through spectrum sharing. For example, International Telecommunication Union Recommendation ITU-R RA.769-2 [4] indicates that above about 40 MHz sharing may be practicable with services in which the transmitters are not in direct line-of-sight of the observations. Notice, however, that astronomical objects are distantly far away and thus their signals are very weak, typically tens of decibels below the noise floor. Therefore, compared with active communication services, astronomical signals are highly vulnerable to interference. As a result, robust signal processing techniques supporting coexistence between radio astronomical observation and wireless communications is in urgent need.

While radio telescope systems are carefully designed and operated, they often suffer from model mismatch, particularly as the antennas are continuously adjusted to steer their beams towards the astronomical sources of interest as the Earth rotates on its orbit. Each antenna has its own directional response with its gain and phase which may be inaccurately calibrated. Moreover, the propagation of astronomical signals through the atmosphere and ionosphere causes additional perturbation and phase delays to the array with a very long baseline [5]. Therefore, array calibration and robust beamforming against array response distortions in radio astronomy have been important objectives in the past decades [6] [7].

More specifically, a number of robust adaptive beamforming methods have been proposed to address the model mismatch problem. For instance, diagonal loading [8] is a widely used robust adaptive beamforming technique. However, it is difficult to choose an optimal loading factor in different scenarios. Worst-case performance optimization technique [9] makes use of the uncertain set of the steering vector. However, the required *a prior* knowledge about the mismatch vector or the upper bound is hard to obtain in practice. Either overestimation or underestimation of the upper bound would compromise the performance.

In this paper, we propose a robust radio astronomical imaging method to ensure the astronomical imaging quality in the presence of calibration error and strong wireless communication interference by combining the techniques of steering vector estimation and adaptive beamforming. Simulation results clearly demonstrate the effectiveness of the proposed technique by comparing with classical astronomical imaging techniques. As such, the proposed method is considered a suitable technique to perform radio astronomical imaging under coexistence with wireless communications.

Notation : Lower-case (upper-case) bold characters are used to denote vectors (matrices). $\boldsymbol{I}_N$ denotes the $N \times N$ identity matrix. $(\cdot)^{\mathrm{T}}$ and $(\cdot)^{\mathrm{H}}$ denote the transpose and Hermitian operations of a matrix or vector, respectively. Diag$(\cdot)$ denotes a diagonal matrix with the elements of a vector constituting the diagonal entries, whereas diag$(\cdot)$ denotes a vector consists of the diagonal elements of a general matrix.

II. SIGNAL MODEL

A. Background

Modern radio astronomical telescopes commonly use multiple antennas to construct astronomical images based on the principle of radio interferometry [10]. Examples linclude various radio telescopes, such as the Cambridge Radio Telescope, the Very Large Array (VLA) [11], the Westerbork Synthesis Radio Telescope (WSRT) [12], the Square Kilometer Array (SKA) and the Low-Frequency Array (LOFAR), the Allen Telescope Array (ATA), the Long Wavelength Array (LWA), and the Atacama Large Millimeter Array (ALMA). As the Earth rotates, the array aperture observed at different time epochs can be used for array aperture synthesis. As shown
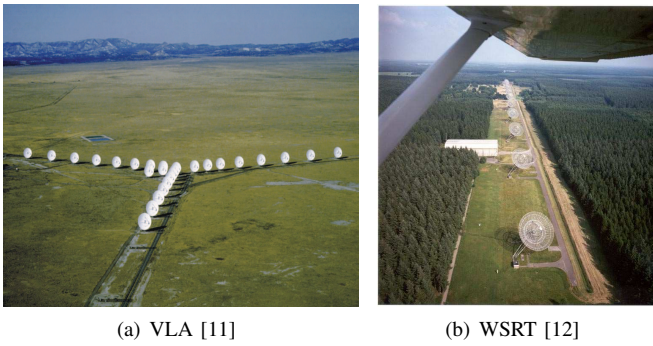
(a) VLA [11]   (b) WSRT [12]
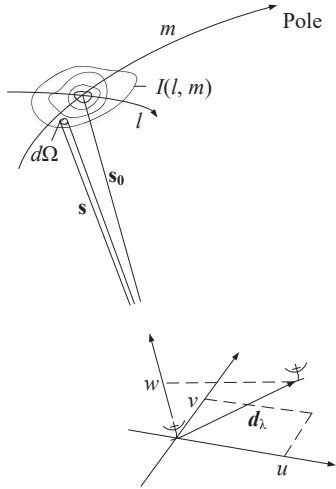
Fig. 1: The VLA and the WSRT.

Fig. 2: Geometric relationship between a source under observation $I(\ell, m)$ and an interferometer or one antenna pair of an array.

in Fig. 1, the structure of the array can be either linear or planar.

We use two coordinate systems respectively for the telescope array and the astronomical objects as shown in Fig. 2 [13]. The vector baseline $\boldsymbol{d}_\lambda$ with components in coordinate system (u, v, w) connects each pair of antennas, measured in wavelength. The component w is measured in the direction $\boldsymbol{s}_0$, which is the phase reference position. Components u and v are measured in a plane normal to the direction of the phase reference position. The coordinate system (ℓ, m) corresponds to the projection of the celestial sphere onto a plane that is a tangent at the filed center, measured in radians.

Radio astronomical imaging is based on the correlation of the received signals, obtained from the radio telescope array. Considering D astronomical point sources in a specific observation area of interest, the source intensity is expressed as

$$I(\ell, m) = \sum_{d=1}^{D} I(\ell_d, m_d)\delta(\ell - \ell_d)\delta(m - m_d), \quad (1)$$

where $I(\ell_d, m_d), d = 1, \cdots, D$, denotes the source intensity at position (ℓ_d, m_d), and $\delta(\cdot)$ denotes the Dirac delta function.

B. Visibility Matrix Formulation

In order to estimate the intensity $I(\ell, m)$ based on the signal received at the telescope array, we measure the "visibility", which is depicted as the correlation between different telescope antenna pairs. The visibility is expressed as $V(u_{ij}^k, v_{ij}^k)$, where u_{ij}^k and v_{ij}^k respectively stand for the baseline (the vector connects antenna i and antenna j) components at time epoch t_k in two orthogonal coordinate axes in the Earth surface. The geometric delay is assumed to be compensated. Under certain approximations, such as a planar array and a small field of view, the visibility and the astronomical source intensity are associated for uncorrelated source points with the two-dimensional Fourier transform, expressed as [14]

$$V(u_{ij}^k, v_{ij}^k) = \sum_{d=1}^{D} I(\ell_d, m_d)e^{-2\pi j(u_{ij}^k \ell_d + v_{ij}^k m_d)}, \quad (2)$$

where $j = \sqrt{-1}$ is the imaginary unit. Selecting a reference point at one of the antennas and denoting its coordinate as (u_0^k, v_0^k), we have

$$V(u_{ij}^k, v_{ij}^k) = \sum_{d=1}^{D} e^{-2\pi j(u_{i,0}^k \ell_d + v_{i,0}^k m_d)} I(\ell_d, m_d)$$
$$\cdot e^{-2\pi j(u_{j,0}^k \ell_d + v_{j,0}^k m_d)}. \quad (3)$$

In a matrix form, equation (3) is rewritten as

$$\boldsymbol{R}_k = \boldsymbol{A}_k \boldsymbol{B} \boldsymbol{A}_k^{\mathrm{H}}, \quad (4)$$

where $\boldsymbol{A}_k = [\boldsymbol{a}_k(\ell_1, m_1), \cdots, \boldsymbol{a}_k(\ell_D, m_D)]$ denotes the telescope array steering matrix at a given time epoch t_k due to the geometrical delays associated with the array and source geometry. The array steering vector associated with the d-th source, located at (ℓ_d, m_d), is expressed as

$$\boldsymbol{a}_k(\ell_d, m_d) = \left[e^{-j2\pi(u_1^k \ell_d + v_1^k m_d)}, \cdots, e^{-j2\pi(u_P^k \ell_d + v_P^k m_d)}\right]^{\mathrm{T}}, \quad (5)$$

where P denotes the number of antennas in the telescope array. In addition, $\boldsymbol{B} = \mathrm{Diag}\left[I(\ell_1, m_1), \cdots, I(\ell_D, m_D)\right]$ is a diagonal matrix representing the intensity of the point sources.

In practice, the array received signal consists of additive system noise. Assume independent and identically distributed (i.i.d), additive white Gaussian noise on each antenna with variance σ_n^2. Then, equation (4) can be rewritten as

$$\tilde{\boldsymbol{R}}_k = \boldsymbol{A}_k \boldsymbol{B} \boldsymbol{A}_k^{\mathrm{H}} + \sigma_n^2 \boldsymbol{I}_P. \quad (6)$$

III. PROBLEM FORMULATION

With rapid increases in technological innovation, the demand for wireless broadband has soared. This demand would require a shared spectrum utilization of the frequency bands, that have traditionally slated for radio astronomy, with other applications, such as broadcasting and cellular communications. As a result, radio telescope signals will be increasingly contaminated by various radio frequency interference sources from broadcast and cellular communications signals. Different from astronomical signals, which are distant far-filed and are located in the array mainlobe, the interferers are usually located in the near-field and enter the telescope antennas through the sidelobes. As the Earth rotates, the sidelobe levels may vary over time as the antennas adjust their main beams

towards the imaged direction. Therefore, the corresponding array response vectors for the interferers are typically time-varying.

Assuming Q interferers, the covariance matrix of the interference signals at time epoch t_k is expressed as

$$\boldsymbol{R}_k^i = \boldsymbol{A}_k^i \boldsymbol{B}_k^i (\boldsymbol{A}_k^i)^{\mathrm{H}}, \tag{7}$$

where the superscript i is used to represent the interference. In addition, $\boldsymbol{A}_k^i = [\boldsymbol{a}_{1k}^i, \cdots, \boldsymbol{a}_{Qk}^i]$ is the array response matrix of the Q interferers, where $\boldsymbol{a}_{qk}^i$ is the spatial signature of the q-th interfering source at time epoch t_k, $q = 1, \cdots, Q$. $\boldsymbol{A}_k^i$ and $\boldsymbol{R}_k^i$ are usually short-time stationary (in the order of 10 ms) [15].

As mentioned above, astronomical observations using a long baseline array would inevitably experience model mismatch due to antenna gain and phase variations that are not perfectly calibrated, and unknown atmospheric and ionospheric disturbances. The model mismatch leads to distortions in the array response over different time epochs. Denote the unknown complex gain matrix as $\boldsymbol{\Gamma}_k = \mathrm{Diag}[\gamma_{1,k}, \cdots, \gamma_{P,k}]$ and the presumed steering vector corresponding to the d-th source at time epoch t_k as $\bar{\boldsymbol{a}}_k(\ell_d, m_d)$. Then, correspondingly, the actual steering vector becomes $\boldsymbol{\Gamma}_k \bar{\boldsymbol{a}}_k(\ell_d, m_d)$. In this case, taking both steering vector mismatch and interference signals into account, the measured visibility matrix becomes [16]

$$\boldsymbol{R}_k = \boldsymbol{\Gamma}_k \bar{\boldsymbol{A}}_k \boldsymbol{B} \bar{\boldsymbol{A}}_k^{\mathrm{H}} \boldsymbol{\Gamma}_k^{\mathrm{H}} + \sigma_n^2 \boldsymbol{I}_P + \boldsymbol{R}_k^i, \tag{8}$$

where $\bar{\boldsymbol{A}}_k = [\bar{\boldsymbol{a}}_k(\ell_1, m_1), \cdots, \bar{\boldsymbol{a}}_k(\ell_D, m_D)]$. Based on the imaging techniques being used, the model mismatch resulted from the calibration errors generally yields blurring in the computed astronomical imaging, whereas the interference, if not effectively suppressed, may generate false images or even obscure the true astronomical sources in the obtained images. Therefore, it is necessary to develop robust astronomy imaging methods which can effectively mitigate the effect caused by radio frequency interference signals in the presence of model mismatch.

IV. ROBUST ASTRONOMY IMAGING

A. Classical Image Formation Methods

The image formation is an inverse problem based on the visibility matrix observed at all baseline antenna positions over the K time epochs. A well-known classical imaging technique is the data-independent delay-and-sum (DAS) beamformer, which estimates the source intensity at all positions within the interested region Ω as [14]

$$I^{\mathrm{DAS}}(\ell, m) = \frac{1}{K} \sum_{k=1}^{K} \bar{\boldsymbol{a}}_k^{\mathrm{H}}(\ell, m) \hat{\boldsymbol{R}}_k \bar{\boldsymbol{a}}_k(\ell, m), \forall (\ell, m) \in \Omega. \tag{9}$$

The resulting image is usually referred to as a dirty image due to image smearing because the image resolution is limited by the array aperture.

In order to improve the image quality in the presence of interference, several adaptive beamforming techniques have been used for radio astronomical imaging. Among them, two adaptive beamformers are commonly used, namely, the minimum variance distortionless response (MVDR) beamformer [17] and the adapted angular response (AAR) beamformer

[18]. The MVDR beamformer, also known as the Capon beamformer, is given as

$$I^{\mathrm{MVDR}}(\ell, m) = \sum_{k=1}^{K} \frac{1}{\bar{\boldsymbol{a}}_k^{\mathrm{H}}(\ell, m) \hat{\boldsymbol{R}}_k^{-1} \bar{\boldsymbol{a}}_k(\ell, m)}, \tag{10}$$

whereas the AAR beamformer is expressed as

$$I^{\mathrm{AAR}}(\ell, m) = \frac{\displaystyle\sum_{k=1}^{K} \bar{\boldsymbol{a}}_k^{\mathrm{H}}(\ell, m) \hat{\boldsymbol{R}}_k^{-1} \bar{\boldsymbol{a}}_k(\ell, m)}{\displaystyle\sum_{k=1}^{K} \bar{\boldsymbol{a}}_k^{\mathrm{H}}(\ell, m) \hat{\boldsymbol{R}}_k^{-2} \bar{\boldsymbol{a}}_k(\ell, m)}. \tag{11}$$

Note that the DAS, MVDR, and AAR beamformers all suffer performance degradation in the presence of model mismatch.

B. Robust Image Formation Method

In this section, we propose a robust astronomy imaging method which can effectively achieve interference cancellation in the presence of steering vector mismatch.

Considering the d-th source at time epoch t_k, for notational simplicity, we omit (ℓ_d, m_d) and k in the sequel. Using the MVDR beamformer, we maximize the beamformer output power as follows:

$$\max_{\boldsymbol{a}} \quad p(\boldsymbol{a}) = \frac{1}{\boldsymbol{a}^{\mathrm{H}} \hat{\boldsymbol{R}}^{-1} \boldsymbol{a}}, \tag{12}$$

which is equivalent to minimize $\boldsymbol{a}^{\mathrm{H}} \hat{\boldsymbol{R}}^{-1} \boldsymbol{a}$. An apparent but undesired solution is $\boldsymbol{a} = \boldsymbol{0}$. To avoid this result, we utilize the presumed steering vector $\bar{\boldsymbol{a}}$. Denote $\boldsymbol{a} = \boldsymbol{\Gamma} \bar{\boldsymbol{a}} = \bar{\boldsymbol{a}} + \boldsymbol{e}$. Note that the actual steering vector $\boldsymbol{a}$ must not converge to any interference region [19]. Then, the optimization problem of searching for the actual steering vector $\boldsymbol{a}$ can be formulated to search for its mismatch vector $\boldsymbol{e} = \boldsymbol{a} - \bar{\boldsymbol{a}}$ as follows:

$$\min_{\boldsymbol{e}} \quad (\bar{\boldsymbol{a}} + \boldsymbol{e})^{\mathrm{H}} \hat{\boldsymbol{R}}^{-1} (\bar{\boldsymbol{a}} + \boldsymbol{e}) \tag{13}$$

$$\text{s.t.} \quad (\bar{\boldsymbol{a}} + \boldsymbol{e})^{\mathrm{H}} \hat{\boldsymbol{R}} (\bar{\boldsymbol{a}} + \boldsymbol{e}) \leq \bar{\boldsymbol{a}}^{\mathrm{H}} \hat{\boldsymbol{R}} \bar{\boldsymbol{a}},$$

where the inequality constraint is introduced to guarantee the estimated signal steering vector not converging to any interferes.

In order to avoid the undesired solution $\boldsymbol{e} = -\bar{\boldsymbol{a}}$, we decompose the mismatch vector $\boldsymbol{e}$ into two components: one is $\boldsymbol{e}_\perp$, which is orthogonal to the presumed steering vector $\bar{\boldsymbol{a}}$, and the other is $\boldsymbol{e}_\parallel$, which is parallel to $\bar{\boldsymbol{a}}$. Since $\boldsymbol{e}_\parallel$ is a scaled replica of the presumed steering vector, it does not affect the output signal-to-interference-plus-noise ratio and the resulting image quality. Therefore, instead of estimating $\boldsymbol{e}$, only the orthogonal component $\boldsymbol{e}_\perp$ needs to be obtained. Thus, the optimization problem (13) can be reformulated as

$$\min_{\boldsymbol{e}_\perp} \quad (\bar{\boldsymbol{a}} + \boldsymbol{e}_\perp)^{\mathrm{H}} \hat{\boldsymbol{R}}^{-1} (\bar{\boldsymbol{a}} + \boldsymbol{e}_\perp) \tag{14}$$

$$\text{s.t.} \quad \bar{\boldsymbol{a}}^{\mathrm{H}} \boldsymbol{e}_\perp = 0,$$

$$(\bar{\boldsymbol{a}} + \boldsymbol{e}_\perp)^{\mathrm{H}} \hat{\boldsymbol{R}} (\bar{\boldsymbol{a}} + \boldsymbol{e}_\perp) \leq \bar{\boldsymbol{a}}^{\mathrm{H}} \hat{\boldsymbol{R}} \bar{\boldsymbol{a}},$$

which is a quadratically constrained quadratic programming (QCQP) problem. Its solution is always feasible and can be obtained by using convex optimization software [20]. As such, the actual steering vector is estimated. This, in turn, allows
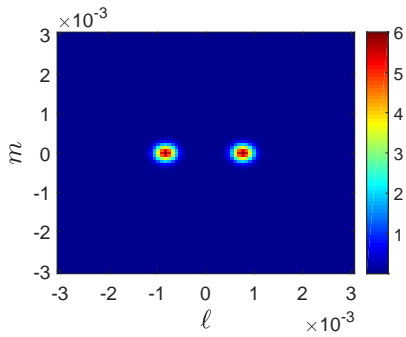
Fig. 3: The simulated true image.

robust astronomical imaging by using the MVDR or AAR beamforming technique.

To summarize, in the proposed method, robust astronomical imaging is achieved by performing the following two steps for each pixel (ℓ, m) in the region of interest and at each time epoch t_k:

Step 1: Estimate the actual steering vector $\boldsymbol{a}_k(\ell, m)$ that corrects the presumed steering vector $\bar{\boldsymbol{a}}_k(\ell, m)$ by solving the constrained optimization problem (14);

Step 2: Generate the MVDR or AAR dirty image, respectively described in (10) and (11), where the presumed steering vector $\bar{\boldsymbol{a}}_k(\ell, m)$ is replaced by the estimated actual steering vector $\boldsymbol{a}_k(\ell, m)$.

V. SIMULATION RESULTS

In this section, we provide simulation results to demonstrate the imaging performance of the proposed astronomical imaging method and compare the results without using QCQP. Throughout this section, the VLA telescope with $P = 27$ antennas is used as the array configuration. An 8-hour observation time period with 695 time epochs is considered. The simulated sky region, shown in Fig. 3, contains two elliptical Gaussian sources. The signal-to-noise ratio (SNR) of each source is assumed to be -30 dB. The perturbation $\boldsymbol{\Gamma}_k$ on the steering vector is described as Gaussian random variables with $\text{diag}(\boldsymbol{\Gamma}_k) \sim \mathcal{CN}(\mathbf{1}, \sigma^2 \boldsymbol{I})$ with $\sigma^2 = 1.44$. Two independent terrestrial interferences are assumed, with input interference-to-noise ratio to be 30 dB and 40 dB, respectively. The interference steering vectors are assumed to vary independently over the time epochs as $\boldsymbol{a}_{qk}^i \sim \mathcal{CN}(\mathbf{0}, \boldsymbol{I})$.

In Fig. 4, the three plots in the first row show results with no array model mismatch, whereas the last six plots are obtained in the presence of array model mismatch. Fig. 4(a) shows the dirty image generated by the classical DAS method. It is clear that, because DAS does not suppress interference signals, the interference dominates the resulting image and the astronomical sources are completely obscured. The effects of interference contamination can be reduced by the two adaptive beamforming methods, and the results obtained from the MVDR and AAR methods are shown in Fig. 4(b) and Fig. 4(c), respectively. Both achieve good interference suppression capability and the sources are clearly revealed.

The second row of Fig. 4 shows results of the DAS, MVDR, and AAR imaging techniques in the presence of model mismatch. In this case, both the MVDR and AAR dirty images

exhibit degradations, as respectively shown in Fig. 4(e) and Fig. 4(f). Particularly, the dirty image obtained from the AAR method is significantly distorted as the peak values of the distortion appear around the true source positions.

The third row of Fig. 4 shows the results when the estimated actual steering vector obtained from the proposed technique is applied. We can notice that the proposed method could effectively mitigate the effects of the model mismatch error, especially for the AAR method. With the use of the proposed method, the MVDR and AAR dirty images obtained in the presence of model mismatch are more consistent with their corresponding counterparts when generated without model mismatch. Note also that the dynamic image range is increased in the third row with the use of the proposed technique, compared with the second row.

VI. CONCLUSION

In this paper, we proposed a robust astronomical imaging technique for radio frequency interference cancellation in the presence of array model mismatch. The proposed technique is based on the estimation of the actual steering vector by solving a QCQP problem. The estimated actual steering vector is then used in the conventional adaptive beamforming methods applied for radio astronomical imaging. Simulation results show that the proposed method, particularly that based on the AAR beamformer, achieves significant improvement in the resulting imaging performance as compared to the conventional AAR or MVDR without array steering vector correction.

REFERENCES

[1] S. Hall, "How astronomy benefits society and humankind," *Universe Today*, Nov. 2013. Available at http://www.universetoday.com/106302/how-astronomy-benefits-society-and-humankind/

[2] W. van Driel, "Radio quiet, please! – Protecting radio astronomy from interference," in *Proc. IAU Symposium*, vol. 260, pp. 457-464, 2009.

[3] T. E. Gergely, "Spectrum access for the passive services: The past and the future," *Proc. IEEE.*, vol. 102, no. 3, pp. 393–398, Mar. 2014.

[4] International Telecommunication Union, Recommendation ITU-R RA.769-2: Protection Criteria Used for Radio Astronomical Measurements. Available at http://www.itu.int/rec/R-REC-RA.769-2-200305-I.

[5] S. J. Wijnholds, S. van der Tol, R. Nijboer, and A.-J. van der Veen, "Calibration challenges for future radio telescopes," *IEEE Signal Process. Mag.*, vol. 27, no. 1, pp. 30–42, Jan. 2010.

[6] S. Van der Tol and A. J. Van der Veen, "Application of robust Capon beamforming to radio astronomical imaging," *in Proc. IEEE Int. Conf. Acoustics, Speech and Signal Proc. (ICASSP)*, Philadelphia, PA, Mar. 2005.

[7] V. Ollier, M. N. E. Korso, R. Boyer, P. Larzabal, and M. Pesavento, "Robust calibration of radio interferometers in non-Gaussian environment," *arXiv preprint*, arXiv:1612.02023.

[8] H. Cox, R. Zeskind, and M. Owen, "Robust adaptive beam-forming," *IEEE Trans. Acoust. Speech, Signal Process.*, vol. ASSP-35, no. 10, pp. 1365–1376, Oct. 1987.

[9] S. A. Vorobyov, A. B. Gershman, and Z.-Q. Luo, "Robust adaptive beamforming using worst-case performance optimization: A solution to the signal mismatch problem," *IEEE Trans. Signal Process.*, vol. 51, no. 2, pp. 313–324, Feb. 2003.
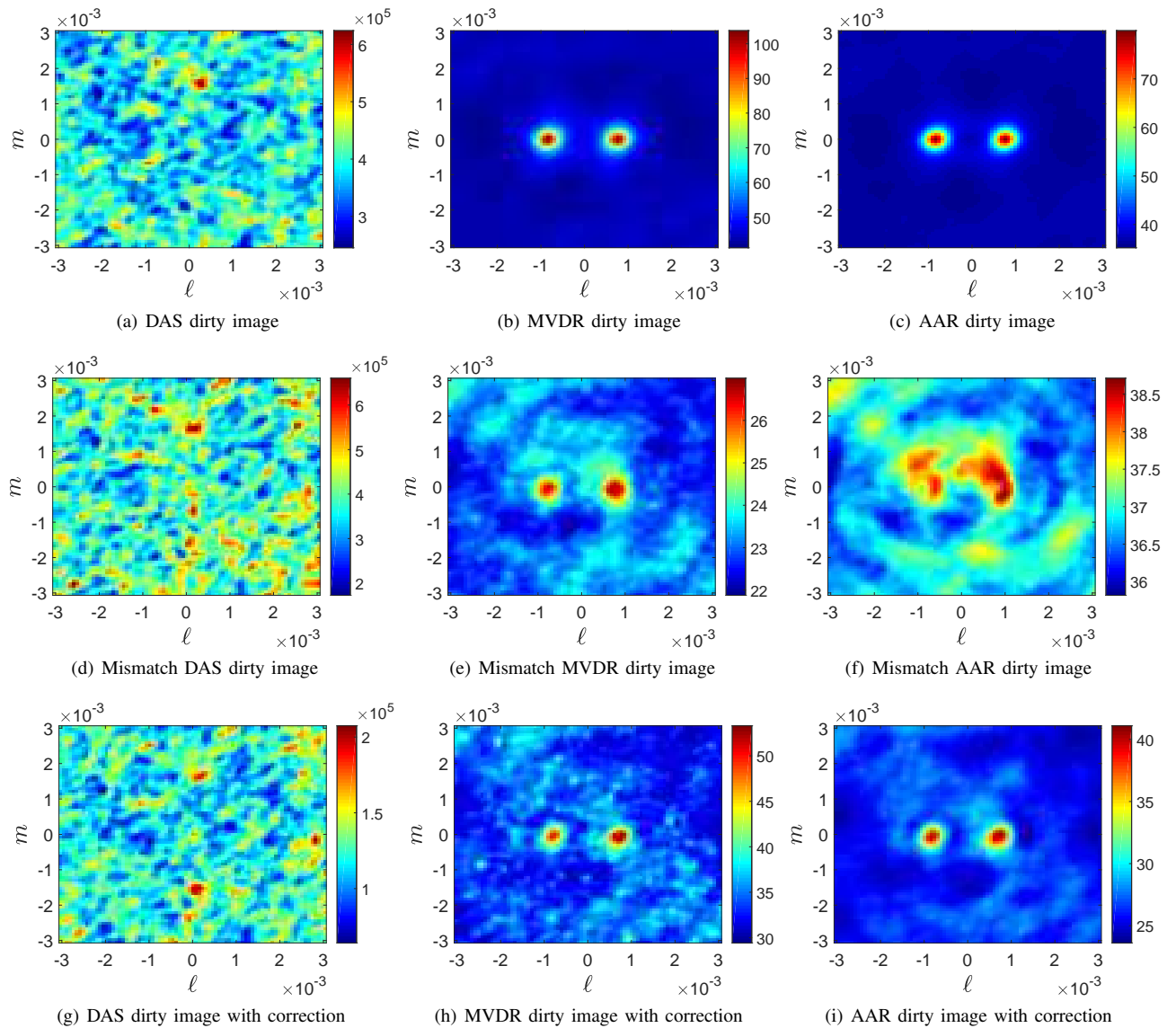
Fig. 4: Comparison of dirty images generated by different beamforming methods. (a), (b) and (c) are generated by the DAS, MVDR, and AAR beamformers without steering vector mismatch; (d), (e), and (f) are generated in the presence of steering vector mismatch by using the presumed steering vector in the DAS, MVDR, and AAR beamformers; (g), (h), and (i) are generated in the presence of steering vector mismatch by using the estimated actual steering vector in the DAS, MVDR, and AAR beamformers.

[10] M. Ryle, "A new radio interferometer and its application to the observation of weak stars," *Proc. Royal Society A*, vol. 211, pp. 351–375, 1952.

[11] Very Large Array website: http://www.vla.nrao.edu.

[12] Westerbork Synthesis Radio Telescope website: https://www.astron.nl/radio-observatory/public/public-0.

[13] A. R. Thompson, J. M. Moran, and G. W. Swenson, *Interferometry and Aperture Synthesis in Radio Astronomy, 2nd Ed.* New York, NY: Wiley, 1986.

[14] R. Levanda and A. Leshem, "Synthetic aperture radio telescopes," *IEEE Signal Process. Mag.*, vol. 27, no. 1, pp. 14–29, Jan. 2010.

[15] A. Leshem, A.-J. van der Veen, and A.-J. Boonstra, "Multichannel interference mitigation techniques in radio astronomy," *Astron. Astrophys. Suppl.*, vol. 126, pp. 161–167, Now. 2000.

[16] A. Leshem and A.-J. van der Veen, "Radio-astronomical imaging in the presence of strong radio interference," *IEEE Trans. Info. Theory*, vol. 46, pp. 1730–1747, 2000.

[17] A.-J. van der Veen, A. Leshem, and A.-J. Boonstra, "Signal processing for radio astronomical arrays," in *Proc. IEEE Sensor Array and Multichannel Signal Processing Workshop*, Stiges, Spain, July 2004, pp. 1–10

[18] C. Ben-David and A. Leshem, "Parametric high resolution techniques for radio astronomical imaging," *IEEE J. Sel. Topics Signal Process.*, vol. 2, pp. 670–684, Oct. 2008.

[19] Y. Gu and A. Leshem, "Robust adaptive beamforming based on interference covariance matrix reconstruction and steering vector estimation," *IEEE Trans. Signal Process.*, vol. 60, no. 7, pp. 3881–3885, Jul. 2012.

[20] M. Grant, S. Boyd, and Y. Ye, "CVX: MATLAB software for disciplined convex programming," 2009. Available: http://www.stanford.edu/ boyd/cvx.